Role of Charged Residues at the OmpF Porin Channel Constriction Probed by Mutagenesis and Simulation[†,‡]

Prashant S. Phale,[§,||] Ansgar Philippsen,[⊥] Christine Widmer,[§] Vrishali P. Phale,[§] Jurg P. Rosenbusch,[§] and Tilman Schirmer*[,⊥]

Division of Microbiology, Biozentrum, University of Basel, Klingelbergstrasse 70, CH-4056 Basel, Switzerland, and Division of Structural Biology, Biozentrum, University of Basel, Klingelbergstrasse 70, CH-4056 Basel, Switzerland

Received January 8, 2001; Revised Manuscript Received March 6, 2001

ABSTRACT: The channel constriction of OmpF porin, a pore protein in the bacterial outer membrane, is highly charged due to the presence of three arginines (R42, R82, and R132) and two acidic residues (D113 and E117). The influence of these charges on ion conductance, ion selectivity, and voltage gating has been studied with mutants D113N/E117Q, R42A/R82A/R132A/D113N/E117Q, and V18K/G131K, which were designed to remove or add protein charge at the channel constriction. The crystal structures revealed no or only local changes compared to wild-type OmpF, thus allowing a comparative study. The single-channel conductance of the isosteric D113N/E117Q variant was found to be 2-fold reduced, and that of the pentuple mutant was 70% of the wild-type value, despite a considerably larger pore cross section. Ion selectivity was drastically altered by the mutations with cation/anion permeability ratios ranging from 1 to 12. Ion flow through these and eight other mutants, which have been characterized previously, was simulated by Brownian dynamics based on the detailed crystal structures. The calculated ion selectivity and relative channel conductance values agree well with the experimental data. This demonstrates that ion translocation through porin is mainly governed by pore geometry and charge, the two factors that are properly represented in the simulations.

OmpF porin, a membrane protein of *Escherichia coli* which confers permeability to the outer membrane (for reviews, see refs *1*−*3*), is one of the few channels with known three-dimensional structure (*4*). The ease with which it can be genetically modified, overexpressed (*5*), crystallized (*6*), and functionally characterized (*7*, *8*) renders this system ideally suited for detailed investigations of structure−function relationships, in particular with respect to the determinants of ion flow through transmembrane channels.

Each of the three channels of the trimeric protein is surrounded by a 16-stranded antiparallel β-barrel. About halfway through the membrane the lumen is narrowed by the internal loop L3 (Figure 1). The constriction of the hourglass-shaped channel is lined almost exclusively by ionizable residues, with basic residues at one side and acidic residues on the other across the channel. This arrangement, which is also found in the other nonspecific porins of known structure (*9*−*12*), results in a strong electrostatic field parallel to the plane of the membrane (*13*). When incorporated into planar lipid bilayers, OmpF exhibits large single-channel conductance steps, moderate cation selectivity, and voltage-induced gating (*8*). Interestingly, the homologous phosphoporin (PhoE), which is expressed under phosphate limitation, shows a preference for anions, although the structure is closely related (*4*). The difference has been attributed to the presence of additional lysine residues at the channel lining (*14*).

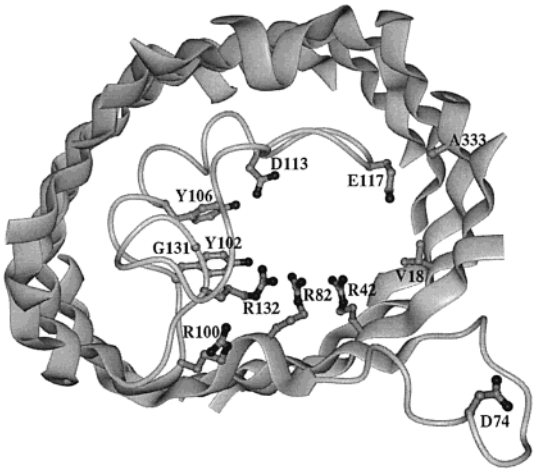

FIGURE 1: Structure (*4*) of the channel constriction in wild-type OmpF porin. View from the extracellular side onto the monomer with strands depicted as broad ribbons and loops L2 and L3 as narrow tubes. The model has been clipped to allow a full view of the constriction. D74 is part of loop L2 that latches into an adjacent monomer (not shown) of the trimer (see also ref *18*). Wild-type residues that have been altered by site-directed mutagenesis are shown as labeled ball-and-stick models. The figure was produced with DINO (*38*).

[†] This work was supported by grants from the Swiss National Science Foundation to J.P.R. and T.S.

[‡] The crystallographic coordinates have been deposited in the Protein Data Bank as entries 1hxt, 1hxu, and 1hxx.

* To whom correspondence should be addressed. Phone: +41-61-2672089. Fax: +41-61-2672109. E-mail: tilman.schirmer@unibas.ch.

[§] Division of Microbiology, Biozentrum, University of Basel.

[||] Current address: Biotechnology Center, Indian Institute of Technology, Bombay Powai, Mumbai 400 076, India.

[⊥] Division of Structural Biology, Biozentrum, University of Basel.

10.1021/bi010046k CCC: $20.00 © 2001 American Chemical Society
Published on Web 05/03/2001

Several OmpF mutants have been produced previously, either by selection (*15*, *16*) or by site-directed mutagenesis (*5*, *8*, *17*, *18*). X-ray structure analyses (*16*−*19*) demonstrated the robustness of the porin architecture, which allows residue replacements at the channel lining or even deletions in the internal loop without compromising the protein fold. Replacement of charged residues at the pore constriction altered ion selectivity in the expected directions (*8*, *16*, *18*). The mechanism of voltage and pH gating is still unresolved. A large-scale movement of L3 (*20*), however, can be ruled out, since tethering this loop to the barrel wall by means of a disulfide link did not abolish channel closing (*17*, *21*, *22*).

To relate channel structure to electrophysiological function, molecular simulations are needed. For wide pores, Brownian dynamics simulations (*23*) taking into account the detailed geometry of the pore and the derived electrostatic potential within the lumen have proven to be valuable in computing ion trajectories (*24*). Since this mean field method does not consider explicitly detailed molecular interactions and protein dynamics, large numbers of trajectories can be computed in a reasonable time and statistically significant transfer efficiencies can be obtained. In a first study, Schirmer and Phale (*25*) have applied Brownian dynamics to derive cation and anion permeabilities through OmpF, PhoE, OmpK36, and two OmpF mutants. It was shown that the highly charged dipolar channel constriction serves to enhance ion permeability. The good correlation between simulated relative channel conductance and ion selectivity with the experimental values demonstrated that the essential determinants of ion translocation through porins were captured. Recently, the method has been developed further to implement boundary conditions of concentration and transmembrane potential and to allow for ion−ion interactions within the channel (*26*). In a first test, the algorithm was applied to the OmpF channel (*26*).

In this study, the effects of drastic changes in the charge constellation at the OmpF pore constriction have been investigated by crystallographic and functional characterization of three site-directed mutants. Ion flow through these pores and through eight other OmpF mutant pores, characterized previously, has been simulated by Brownian dynamics. The results are compared with measured single-channel conductance and ion selectivity values.

MATERIALS AND METHODS

Mutagenesis, Overexpression, and Purification. Porin mutants were constructed by site-directed mutagenesis and overexpressed in the porin deficient *E. coli* strain BL21-(DE3)omp8 as described previously (*5*). The proteins were purified according to an established protocol (*8*, *17*) with negative extraction in SDS[1] followed by selective extraction and purification in octyl-POE detergent using chromatofocusing and gel filtration chromatography. The final yield was 1−2 mg of homogeneous protein per gram of cell mass (wet weight).

Functional Assays. The electrophysiological properties of the porin variants were determined after reconstitution into planar lipid bilayers as described previously (*8*). All mutant proteins inserted into the bilayer with efficiency like that of the wild type. The baths contained 1 mM $CaCl_2$, 10 mM Tris (pH 7.4), and 1 M NaCl for single-channel conductance measurements. Zero-current potentials were determined after application of a 0.1:1 M NaCl gradient. Ion selectivities (P_{Na}/P_{Cl}) were calculated according to the Goldman−Hodgkin−Katz formalism from the zero-current potentials (*27*). The critical voltage for channel closing (V_c) was determined by application of a 0 to 250 mV voltage ramp within 100 s. Liposome swelling assays were performed as described previously (*8*, *28*). The change in optical density due to liposome swelling in the presence of various sugars was monitored at a wavelength of 500 nm using a Jasco UV−vis spectrophotometer (model 7850).

X-ray Crystallography. Crystallization was carried out using the microdialysis method as described for the wild-type protein (*6*). OmpF mutant KK was collected at a rotating anode generator; data sets of NQAAA and Y106F were collected at an EMBL beamline of the DESY synchrotron (Hamburg, Germany). Processing and merging was carried out using MOSFLM and SCALA from the CCP4 suite (*29*). The structures were determined by the difference Fourier technique based on the wild-type model. Refinement was performed with REFMAC (*30*) using the maximum likelihood target function. The R_{free} calculation was based on the same set of test reflections as in refinement of wild-type OmpF.

Solvent (ion) accessible cross-sectional areas were determined as a function of the channel *z* coordinate (the direction of the membrane normal defined by the molecular 3-fold axis). For this, the number of those grid points (spacing 0.5 Å × 0.5 Å × 0.5 Å) within a given *x*−*y* section was counted that belonged to the channel and had a distance from the nearest protein atom larger than the probe radius (1.4 Å) plus the van der Waals radius of this protein atom. The semiautomatic C program can be obtained upon request.

Brownian Dynamics Simulation. The UHBD program (*31*), modified to account for planar geometry (*25*), was employed for the simulation of ion translocation through trimeric porin channels. The same geometric setup and parameters as in Schirmer and Phale (*25*) were used. In brief, the dielectric properties of the membrane were modeled by a tripartite slab of low dielectric surrounding the porin trimer, which was centered at the origin and oriented with the molecular symmetry axis (*z*) perpendicular to the membrane. Ions were released on a plane (25 Å × 25 Å) parallel with the membrane at $z = 40$ Å. The reaction criterion was fulfilled for an ion appearing on the other side of the membrane ($z \leq -25$ Å). In the previous study (*25*), a small fraction (<2%) of the trajectories had to be abandoned, because the ions came too close to some protein charges and stayed bound. Here, this artifact caused by the rather coarse spacing (1 Å) of the exclusion grid was circumvented by a slight enlargement (0.3 Å) of the Na^+ and Cl^- crystal radii to 1.2 and 2.1 Å, respectively. A charge of −1 was assigned to the cysteines in mutants R42C and R82C. Hydration of the ions was not modeled. Ion−ion interactions were not taken explicitly into account, but electrostatic screening was modeled by considering the bulk ionic strength. For each porin variant, 5000 Na^+ and 5000 Cl^- trajectories were calculated at ionic strengths of 1 and 0.55 M. From each set of trajectories, the

[1] Abbreviations: SDS, sodium dodecyl sulfate; octyl-POE, octyl polyoxyethylene; *G*, single-channel conductance; P_x, channel permeability for ion x; V_c, critical voltage for channel closure.

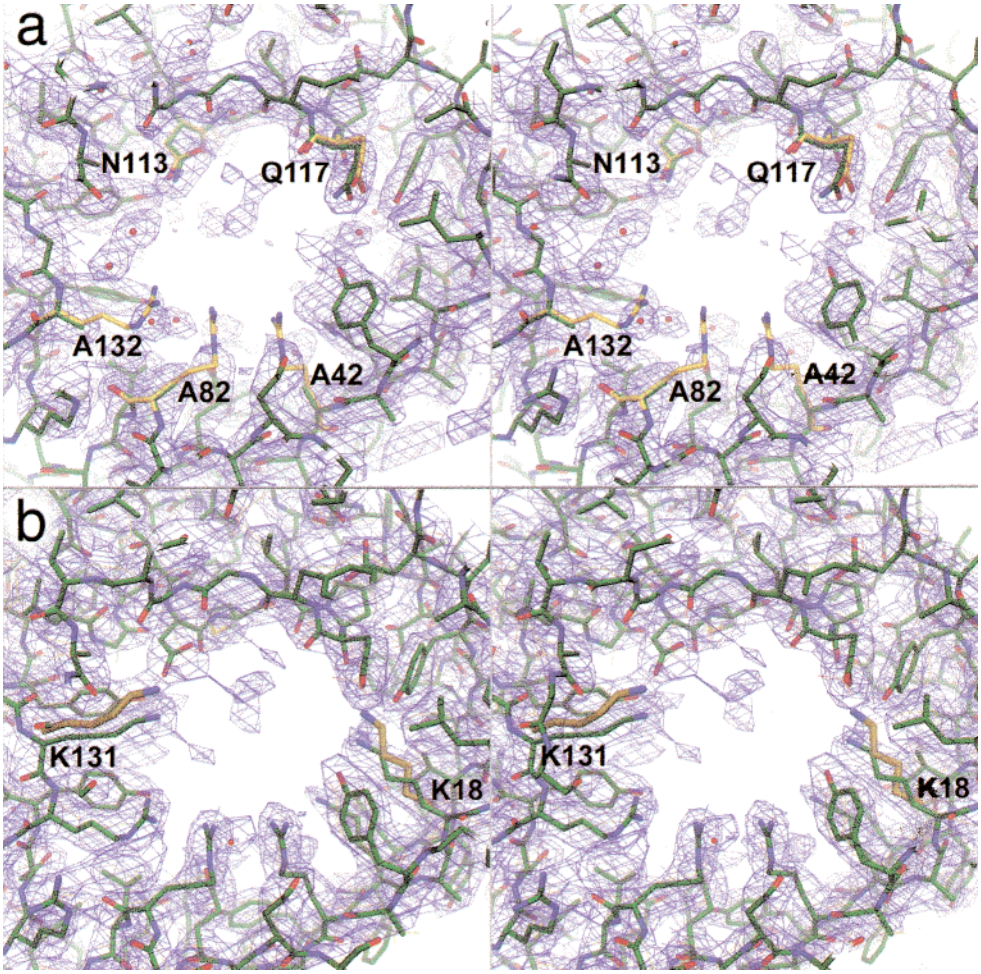

FIGURE 2: Crystal structures of OmpF porin mutants. The final sigmaA weighted $2F_o - F_c$ maps are shown overlaid onto the final models (carbon atoms in green). The mutated residues are labeled. The view is similar to that in Figure 1. (a) For mutant NQAAA, for comparison, OmpF wild-type residues D113, E117, R42, R82, and R132 are shown superimposed with carbon atoms in yellow. (b) For mutant KK, for comparison, residues K18 and K131 of wild-type PhoE are shown superimposed. The figure was produced with DINO (*38*).

positions of the ions were sampled at 10 ps intervals and accumulated in a three-dimensional histogram on a 1 Å × 1 Å × 1 Å grid. This allowed us to determine the number of ions encountered at different z values by appropriate summation in the $x-y$ plane. The transfer efficiency β was defined as the number of productive trajectories per total number of trajectories. The simulation results at 1 M were used to calculate relative conductance ($\beta^+ + \beta^-$) and those at 0.55 M (which is the mean of the two concentrations, 0.1 and 1 M, used in the experiments) to calculate ion selectivity (β^+/β^-).

RESULTS AND DISCUSSION

Pore Constriction with Reduced or No Protein Charge. The pore constriction of wild-type OmpF is lined by three closely spaced arginines (R42, R82, and R132) on one side and carboxyl residues D113 and E117 on the opposite (Figure 1). Part or all of the corresponding protein charges were removed by generating the isosteric single mutant E117Q, the isosteric double mutant NQ (D113N/E117Q), and the pentuple mutant NQAAA (D113N/E117Q/R42A/R82A/R132A). The crystal structure of NQ determined to 3 Å resolution showed virtually no change, when compared with the wild-type structure (data not shown). The crystal structure of NQAAA is shown in Figure 2a, with crystallographic details listed in Table 1. The asparagine and glutamine side chains adopt the same conformation as their wild-type counterparts, whereas truncation of the arginine residues to alanines results in a substantial increase in the solvent (ion) accessible pore cross section by almost 80% (Table 2). The absence of significant changes elsewhere emphasizes the rigidity of the porin backbone structure.

Table 1: Crystallographic Statistics of OmpF Mutants[a]

	KK	NQAAA	Y106F
unit cell (Å)	$a = b = 119.7$, $c = 53.5$	$a = b = 117.1$, $c = 51.3$	$a = b = 118.1$, $c = 52.6$
resolution (Å)	3.0	2.4	2.2
no. of unique reflections	8886	14853	19807
completeness (%)	98.6	93.1	97.9
redundancy	3.6	3.6	3.4
R_{merge} (%)	8.9	7.9	6.5
R (%)	20.0	21.3	17.4
R_{free} (%)	27.0	28.5	24.4
rms deviation			
bond lengths (Å)	0.010	0.010	0.008
bond angles (Å)	0.039	0.033	0.028
mutant − wild type (Å)	0.25	0.25	0.10

[a] The crystals were of space group $P321$.

Single-channel conductance (G) and ion selectivity (P_{Na}/P_{Cl}) of the mutants as measured after incorporation in lipid bilayers are given in Table 2. The single-channel conductance of mutant NQ is only about half of the wild-type OmpF

Table 2: Conductance Properties of OmpF, PhoE, and OmpF Mutants[a]

protein	minimal cross section (%)[b]	conductance G (nS)	P_{Na}/P_{Cl}	critical voltage V_c (mV)
OmpF	100	0.84 ± 0.06	4.5 ± 0.8	145 ± 7
PhoE	70	0.63 ± 0.06	0.44 ± 0.05	135 ± 8
D113G[d]	129	0.80 ± 0.06	1.4 ± 0.1	168 ± 11
E117Q[e]	100[c]	0.64 ± 0.02	2.9 ± 0.2	184 ± 8
E117C/A333C (CC)[f]	109	0.71 ± 0.02	3.0 ± 0.4	191 ± 12
D113N/E117Q (NQ)	94	0.40 ± 0.02	1.0 ± 0.03	102 ± 4
D113N/E117Q/R42A/ R82A/R132A (NQAAA)	177	0.64 ± 0.04	12.3 ± 0.9	113 ± 9
R42C[d]	127	0.78 ± 0.07	9.7 ± 2.0	116 ± 9
R82C[d]	114	0.76 ± 0.06	2.1 ± 0.5 7.6 ± 2.2	107 ± 14
R132P[d]	109	0.77 ± 0.04	13.0 ± 1.9	130 ± 16
R100A[g]	107	0.76 ± 0.02	6.8 ± 0.3	166 ± 14
V18K	100[c]	0.75 ± 0.01	2.6 ± 0.07	165 ± 9
G131K	70[c]	0.76 ± 0.03	3.0 ± 0.3	146 ± 8
V18K/G131K (KK)	75	0.75 ± 0.02	2.1 ± 0.08	113 ± 8
Y102F	100[c]	0.77 ± 0.03	5.1 ± 0.6	192 ± 12
Y106F	93	0.76 ± 0.03	4.1 ± 0.15	206 ± 16
D74A[g]	104	0.82 ± 0.02	4.6 ± 0.3	147 ± 5

[a] G is the mean of typically 100−300 single-conductance step measurements. P_{Na}/P_{Cl} was determined from at least four different membrane preparations. V_c is the mean result of 10−20 experiments using at least three different membrane preparations. [b] Accessible area for a probe with a radius of 1.4 Å; 100% amounts to 31 Å^2. [c] Based on a homology model. [d] From ref *8*. [e] From ref *25*. [f] G and V_c from ref *17*. [g] G and P_{Na}/P_{Cl} from ref *18*.

conductance, and that of NQAAA amounts to 71%. Thus, for these mutants, there is no simple correlation between G and the cross-sectional area (Table 2). Apparently, ion flow is adversely affected by the missing protein charges at the constriction (see below).

Permeation rates of uncharged solutes were measured by monitoring the swelling of proteoliposomes. Due to variation in liposome size and incorporation efficiency, it is not possible to compare the results obtained for different preparations (mutants) directly. Therefore, the results for the different mutants are given relative to the permeation rate of arabinose. It is assumed that the translocation rates of this small sugar are affected least by the alterations at the pore constriction.

Figure 3 shows that monosaccharides translocate only slightly if at all better through the NQAAA mutant pore than through the wild type, while the relative permeation rate for disaccharides is increased 8-fold. Thus, in contrast to conductance, disaccharide rates correlate with channel size. Even though only qualitative, the relative disaccharide rate seems to be a reliable measure of pore size as can be deduced from inspection of a larger body of data. The increased pore size of R132P, D113G, and the two-loop L3 deletion mutants (*17*, *19*), as well as the reduced size of PhoE (*4*) and the KK mutant (see below), correlate with the respective swelling rates (Figure 3). In this context, the reduced ion conductance of both deletion mutants [Supporting Information (*8*, *17*)] is intriguing. It has been suggested that this could be due to increased mobility of the remaining part of the internal loop that would partly obstruct the pore (*8*). In light of the results presented above, the absence of an acidic residue in each of the mutants (D113 in Δ109−114 and E117 in Δ116−120) may also be relevant for their reduced conductance.

Ion selectivity is critically affected by the charge constellation at the pore constriction. This has been observed in several cases previously (*8*, *16*, *18*, *32*, *33*) and was found also in Brownian dynamics simulations (*25*). The change in ion selectivity by a factor of more than 4 for the double mutant NQ (Table 2) is the largest observed so far as a result

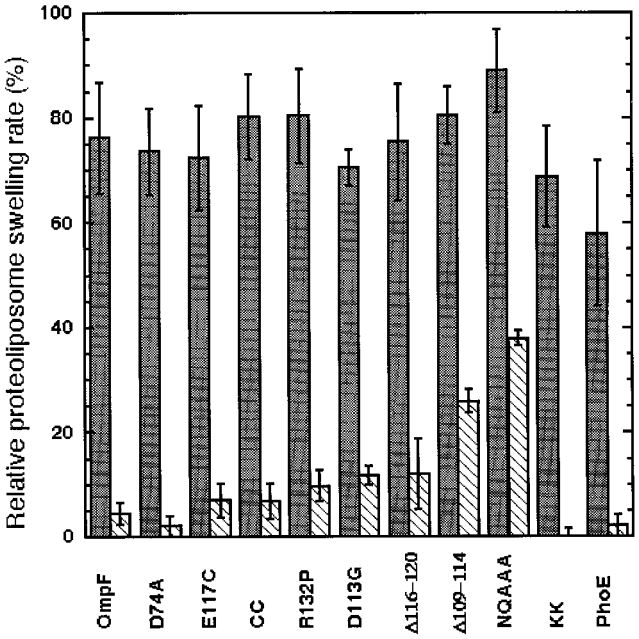

FIGURE 3: Sugar permeation through OmpF, several OmpF mutants, and PhoE as measured by the rate of proteoliposome swelling. The values are normalized to the swelling rate of OmpF proteoliposomes in the presence of arabinose. The dark bars give the mean of the swelling rates for the five monosaccharides (glucose, galactose, mannose, fructose, and *N*-acetylglucosamine); the hatched bars represent the mean rate for four disaccharides (sucrose, lactose, melibiose, and maltose). The error bars represent the variance of the results with three measurements on at least two different liposome preparations per sugar. The full data are given in tabular form as Supporting Information.

of mutagenesis on OmpF. The effect of the two individual substitutions is cumulative as can be seen by comparison with the respective single mutants D113G and E117Q (Table 2). Mutant NQAAA is strongly cation selective, despite the absence of charge at the pore constriction. This must be attributed to the influence of the remaining protein charges at the channel vestibules and to discrimination by ion size.

Phosphoporin-like Pore Constriction. Is it possible to alter functional properties of OmpF porin by introducing additional ionizable residues at its highly charged pore constriction? Guided by the homologous structure of phosphoporin [PhoE (*4*)], residues V18 and G131 (Figure 1) were changed to lysine, either individually (V18K and G131K) or in combination (KK). All variants expressed well and were analyzed functionally (Table 2 and Figure 3). The KK crystal structure (Figure 2b) shows that both mutated residues are well-defined, adopting positions similar to those in PhoE with a resulting smaller pore size (Table 2). The conductance of the mutants lies between that of OmpF and PhoE.

Cation selectivity was found to be significantly reduced, with the double mutant exhibiting a cumulative effect when compared with the single mutants (Table 2). However, conversion of OmpF into a pore with anion preference, such as PhoE, was not achieved. Probably, the other additional lysines in the channel lumen of PhoE are responsible for the remaining difference between PhoE and KK. Indeed, a prominent influence of K69 in PhoE on selectivity has been reported (*14*).

Voltage Gating. Upon application of an external voltage ramp, the conductance of porin channels decreases above a characteristic voltage, V_c (*8*, *34*). V_c has been measured for all mutants (Table 2 and Supporting Information), with the aim of obtaining insight into the structural determinants of channel closing. Quite unexpectedly, mutants NQAAA and KK exhibit virtually the same V_c, which amounts to 78% of the wild-type value. Thus, removal of as well as increase in charge at the pore constriction renders the pore more voltage sensitive. The sensitivity is similar to that of R42C and R82C, whereas mutant R132P shows a V_c almost like that of the wild type (*8*). This is in stark contrast to charge mutants D113G (*8*), E117Q, and E117C/A333C (*17*), which showed considerably increased V_c values. On the other hand, the double carboxyl mutant (D113N/E117Q) shows the lowest V_c observed for all mutants investigated. Thus, there is no apparent correlation between voltage sensitivity and the charge state of the pore constriction. Even more puzzling, effects that are opposite of those observed in OmpF have been reported for PhoE, where homologous residues were mutated (*32*).

Tyrosine residues 102 and 106 on the internal loop L3 are part of the channel lining (Figure 1). Replacement of each of these residues with phenylalanine increased V_c by 30−40% (Table 2 and Supporting Information). In the wild type, these residues are probably uncharged, since upon mutation the ion selectivity did not change. The crystal structure of Y106F (not shown; see Table 1) revealed no changes apart from the missing hydroxyl group. Thus, a very minor mutation, which should keep the electrostatic potential of the protein unchanged, can substantially alter the sensitivity of OmpF toward an external potential. In summary, after large-scale motions of L3 had been ruled out (*17*, *22*) and the failure to identify a hot spot by extensive mutagenesis (Supporting Information), the question concerning the structural basis of OmpF voltage gating is still open.

Simulation of Ion Flow. Ion flow through OmpF, PhoE, and 10 OmpF mutants was simulated by Brownian dynamics (*23*) to relate electrophysiological properties of the open channel with the three-dimensional structures in a quantitative fashion. At the extracellular side of the porin trimer models,

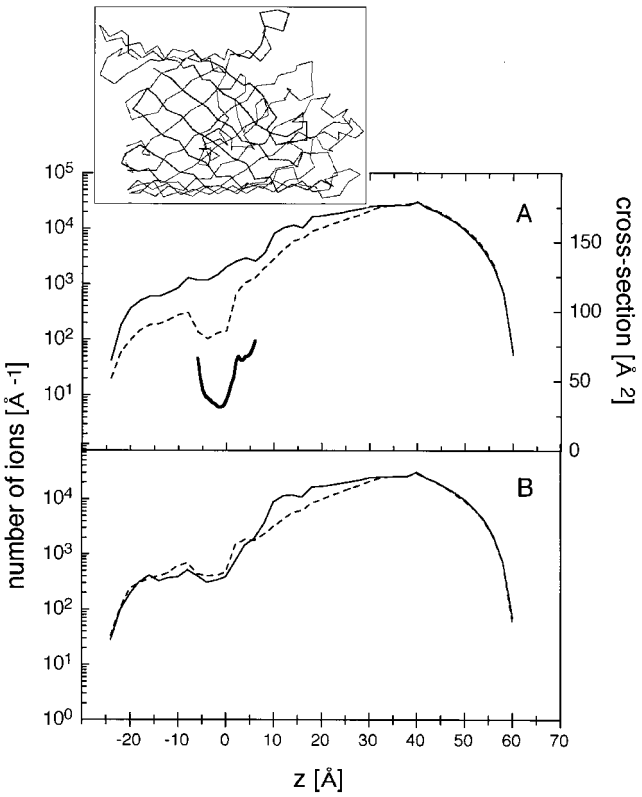

FIGURE 4: Distribution of Brownian dynamics ion trajectories through the pores of wild-type OmpF (A) and OmpF mutant NQ (B). The number of ions [(—) cations and (− − −) anions] as a function of channel coordinate *z* is given as derived from each set of 5000 trajectories that were simulated at an ionic strength of 550 mM. Ions were released at $z = 40$ Å. No normalization with respect to the cross-sectional area of the pore was performed. The profile of the cross-sectional area at the OmpF constriction is given by the bold trace in panel A. The inset shows the C_α trace of one OmpF monomer with the extracellular entrance at the right. The model is properly scaled and aligned with respect to the *z*-axes of the panels.

ions were released one at a time and were allowed to move according to the electrostatic force exerted by the protein charges and a stochastic force representing thermal motion. For detailed views of ion trajectories through OmpF porin, see the preceding study (*25*). From each set of trajectories, the number of ions along the channel coordinate *z* was derived (Figure 4). At the constriction of the OmpF wild-type pore, there is almost no drop in the number of cations, whereas the number of anions is considerably reduced. In the isosteric mutant NQ, this difference is largely abolished. It can be concluded that, for cations, the presence of D113 and E117 in wild-type OmpF counteracts the steric barrier posed by the pore constriction. For the NQAAA mutant, the profiles (not shown) are virtually identical to those of the wild type. Thus, the effect of the reduced potential (five ionizable residues are replaced with neutral residues) is compensated by the increased cross-sectional area.

As in the preceding study (*25*), transfer efficiencies of cations and anions (β_+ and β_-, respectively) were determined, from which relative single-channel conductance and ion selectivity values were deduced. Many of the OmpF variants exhibit only a small change in conductance. This is, within the limits of error, reasonably reproduced by the respective simulations (Figure 5a). Good correlation is found for mutants E117Q and NQ, which have virtually unchanged

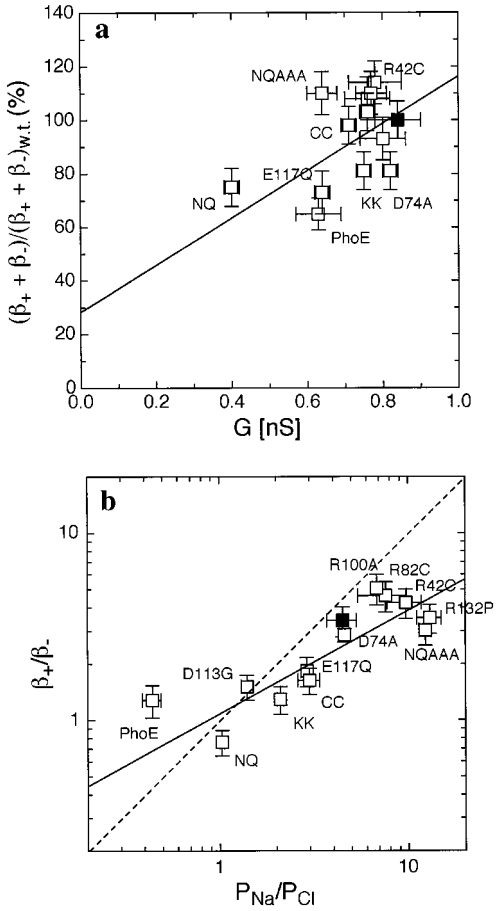

FIGURE 5: Comparison between experimental and simulated electrophysiological properties of OmpF, PhoE, and OmpF mutants (NQ, NQAAA, KK, CC, R42C, R82C, R132P, R100A, D113G, E117Q, and D74A). The wild-type data point is marked by a black square. (a) Scatter plot of the experimental single-channel conductance G (Table 2) vs the sum of the simulated cation and anion transfer efficiencies ($\beta_+ + \beta_-$) normalized to the wild-type value. The linear regression line (correlation coefficient of 0.47) is given. (b) Experimental sodium over chloride selectivity (P_{Na}/P_{Cl}; determined with a 0.1:1 M salt gradient across the membrane) compared with the ratio of simulated cation over anion transfer efficiency (β_+/β_-). The linear regression fit (—) gives a correlation of 0.84. The dashed line represents perfect agreement.

pore geometry, but show drastically reduced conductance (see also above and Table 2). In mutant NQAAA, the increased pore cross section (177%) and the reduced electrostatic potential are counteracting each other. The simulation yields 110% of the wild-type value, whereas the measured value is 76%. The discrepancy may be attributed to the low precision of the simulated conductance value (Figure 5a), but may also be due to systematic errors as discussed in ref *25*.

Taken together, the simulations reproduce the observation that OmpF single-channel conductance is not only determined by physical channel size but also critically dependent on the charge constellation at the channel constriction. The highly charged constriction in wild-type OmpF serves to enhance the local concentration of counterions and, thereby, to increase permeability. The protein charges will also counteract the repulsive dielectric forces (not considered in the simulation) that act on a charge approaching a medium of lower polarizability (*25*, *35*). For porins, however, these have been estimated to be rather small (*25*). The fact that single-channel conductance can be a poor measure of channel size has been realized early; see, for example, ref *36*. In a recent mutant study on porin from *Rhodopseudomonas blastica* (*37*), the influence of protein charge on conductance was less conspicuous, though significant. A linear correlation between conductance and pore size was claimed, but geometrical rather than solvent accessible cross-sectional areas were considered.

The set of porins shows a large variation in ion selectivity that extends over almost 2 orders of magnitude (Table 2 and Figure 5b). Qualitatively, the mutants behave according to expectation. Removal of positive protein charge (R42C, R82C, R132P, and R100A) renders the porin more cation selective, while deletion of negative charge (D113G, CC, and NQ) or placement of additional positive charges (KK) decreases cation selectivity. Since geometric factors cancel out, the simulations directly yield the ion selectivity (β_+/β_-) without any adjustable parameters. As a control, the influence of a charge that is somewhat remote from the pore constriction was tested with mutant D74A (*18*). As expected, truncation of D74 had no influence on the measured or simulated electrophysiological properties of OmpF. There is good correlation between experimental and simulated values (Figure 5b), but for larger values, the simulated selectivities appear to be somewhat underestimated. The discrepancy is small considering the various approximations made, such as independence of ions, using a macroscopic parameter to account for ionic screening also within the channel, neglecting specific protein−ion interactions, and treating the protein as a rigid entity (for further discussion, see ref *25*).

Conclusions. Analysis of a large number of OmpF pore mutants demonstrates that ion conductance is crucially influenced both by the size and by the charge constellation at the channel lining, with an increase in charge density clearly enhancing ion flow. Hereby, and in discriminating cations over anions, the channel constriction plays a strategic role. Application to a large number of mutants has corroborated the validity of Brownian dynamics simulations. They predict faithfully electrophysiological properties and, thus, capture the main determinants of ion translocation through wide transmembraneous pores. Therefore, differential hydration of ions and dielectric forces are less important in porins, in contrast to the situation in specific ion channels.

ACKNOWLEDGMENT

We thank Dr. Bill Montfort for helpful discussions and help in data acquisition. We acknowledge access to EMBL beamline BW7A at the DORIS storage ring, DESY.

SUPPORTING INFORMATION AVAILABLE

Table of electrophysiological properties of OmpF, PhoE, and 34 OmpF mutants and a table of proteoliposome swelling rates induced by 10 different sugars translocating through OmpF, PhoE, and 26 OmpF mutants. This material is available free of charge via the Internet at http://pubs.acs.org.

REFERENCES

1. Schirmer, T. (1998) *J. Struct. Biol. 121*, 101−109.
2. Delcour, A. H. (1997) *FEMS Microbiol. Lett. 151*, 115−123.
3. Schulz, G. E. (1996) *Curr. Opin. Struct. Biol. 6*, 485−490.

4. Cowan, S. W., Schirmer, T., Rummel, G., Steiert, M., Ghosh, R., Pauptit, R. A., Jansonius, J. N., and Rosenbusch, J. P. (1992) *Nature 358*, 727−733.
5. Prilipov, A., Phale, P. S., Van Gelder, P., Rosenbusch, J. P., and Koebnik, R. (1998) *FEMS Microbiol. Lett. 163*, 65−72.
6. Pauptit, R. A., Zhang, H., Rummel, G., Schirmer, T., Jansonius, J. N., and Rosenbusch, J. P. (1991) *J. Mol. Biol. 218*, 505−507.
7. Schindler, H., and Rosenbusch, J. P. (1978) *Proc. Natl. Acad. Sci. U.S.A. 75*, 3751−3755.
8. Saint, N., Lou, K.-L., Widmer, C., Luckey, M., Schirmer, T., and Rosenbusch, J. P. (1996) *J. Biol. Chem. 271*, 20676−20680.
9. Hirsch, A., Breed, J., Saxena, K., Richter, O. M., Ludwig, B., Diederichs, K., and Welte, W. (1997) *FEBS Lett. 404*, 208−210.
10. Weiss, M. S., Kreusch, A., Schiltz, E., Nestel, U., Welte, W., Weckesser, J., and Schulz, G. E. (1991) *FEBS Lett. 280*, 379−382.
11. Dutzler, R., Rummel, G., Alberti, S., Hernandez-Alles, S., Phale, P., Rosenbusch, J., Benedi, V., and Schirmer, T. (1999) *Structure 7*, 425−434.
12. Kreusch, A., and Schulz, G. E. (1994) *J. Mol. Biol. 243*, 891−905.
13. Karshikoff, A., Spassov, V., Cowan, S. A., Ladenstein, R., and Schirmer, T. (1994) *J. Mol. Biol. 240*, 372−384.
14. Bauer, K., Struyve, M., Bosch, D., Benz, R., and Tommassen, J. (1989) *J. Biol. Chem. 264*, 16393−16398.
15. Benson, S. A., Occi, J. L. L., and Sampson, B. A. (1988) *J. Mol. Biol. 203*, 961−970.
16. Jeanteur, D., Schirmer, T., Fourel, D., Simonet, V., Rummel, G., Widmer, C., Rosenbusch, J. P., Pattus, F., and Pages, J.-M. (1994) *Proc. Natl. Acad. Sci. U.S.A. 91*, 10675−10679.
17. Phale, P. S., Schirmer, T., Prilipov, A., Lou, K. L., Hardmeyer, A., and Rosenbusch, J. P. (1997) *Proc. Natl. Acad. Sci. U.S.A. 94*, 6741−6745.
18. Phale, P. S., Philippsen, A., Kiefhaber, T., Koebnik, R., Phale, V. P., Schirmer, T., and Rosenbusch, J. P. (1998) *Biochemistry 37*, 15663−15670.
19. Lou, K.-L., Saint, N., Prilipov, A., Rummel, G., Benson, S. A., Rosenbusch, J. P., and Schirmer, T. (1996) *J. Biol. Chem. 271*, 20669−20675.
20. Watanabe, M., Rosenbusch, J. P., Schirmer, T., and Karplus, M. (1997) *Biophys. J. 72*, 2094−2102.
21. Eppens, E. F., Saint, N., Van Gelder, P., van Boxtel, R., and Tommassen, J. (1997) *FEBS Lett. 415*, 317−320.
22. Bainbridge, G., Mobasheri, H., Armstrong, G. A., Lea, E. J., and Lakey, J. H. (1998) *J. Mol. Biol. 275*, 171−176.
23. Sines, J. J., Allison, S. A., and McCammon, J. A. (1990) *Biochemistry 29*, 9403−9412.
24. Li, S. C., Hoyles, M., Kuyucak, S., and Chung, S. H. (1998) *Biophys. J. 74*, 37−47.
25. Schirmer, T., and Phale, P. (1999) *J. Mol. Biol. 294*, 1159−1168.
26. Im, W., Seefeld, S., and Roux, B. (2000) *Biophys. J. 79*, 788−801.
27. Hille, B. (1992) *Ionic Channels of Excitable Membranes*, Sinauer Associates Inc., Sunderland, MA.
28. Luckey, M., and Nikaido, H. (1980) *Proc. Natl. Acad. Sci. U.S.A. 77*, 167−171.
29. Collaborative computational project number 4 (1994) *Acta Crystallogr. D50*, 760−763.
30. Murshudov, G. N., Vagin, A. A., and Dodson, E. J. (1997) *Acta Crystallogr. D53*, 240−255.
31. Madura, J. D., Briggs, J. M., Wade, R. C., Davies, M. E., Luty, B. A., Ilin, A., Antosiewicz, J., Gilson, M. K., Bagheri, B., Scott, L. R., and McCammon, J. A. (1995) *Comput. Phys. Commun. 91*, 57−95.
32. Van Gelder, P., Saint, N., Phale, P., Eppens, E. F., Prilipov, A., van Boxtel, R., Rosenbusch, J. P., and Tommassen, J. (1997) *J. Mol. Biol. 269*, 468−472.
33. Przybylski, M., Glocker, M. O., Nestel, U., Schnaible, V., Bluggel, M., Diederichs, K., Weckesser, J., Schad, M., Schmid, A., Welte, W., and Benz, R. (1996) *Protein Sci. 5*, 1477−1489.
34. Lakey, J. H., and Pattus, F. (1989) *Eur. J. Biochem. 186*, 303−308.
35. Roux, B., and MacKinnon, R. (1999) *Science 285*, 100−102.
36. Finkelstein, A. (1985) *Ann. N.Y. Acad. Sci. 456*, 26−32.
37. Schmid, B., Maveyraud, L., Kromer, M., and Schulz, G. E. (1998) *Protein Sci. 7*, 1603−1611.
38. Philippsen, A. (2000) http://www.biozentrum.unibas.ch/~xray/dino.

BI010046K